

# Simultaneous Estimation of the Refractive Index and Thickness of Marine Oil Slick from the Degree of Linear Polarization of the Sun-Glint Reflection

Sailing He\* and Hongguang Dong

**Abstract**—Airborne and spaceborne optical remote sensing is an important means for monitoring oil slicks on ocean surface. However, it is still a major challenge to determine both the category (related to a specific value of reflective index) and thickness of the marine oil slick with existing methods, particularly when the oil slick is too thin to obtain significant fluorescence signal with a laser induced fluorescence method. Sun-glint is usually harmful to optical remote sensing of an ocean target. In this work we utilize the polarized sun-glint reflection to monitor oil slicks on a rough ocean surface. The degree of linear polarization (DOLP) of the sun-glint reflection contains the characteristics information of the oil slick with different physical properties. Combining the polarized optical remote sensing and the inversion theory based on a thin-film optical model, we analyze the variation trend of the DOLP with the parameters of solar zenith angle, sensor zenith angle, relative azimuth angle, refractive index and thickness of the oil slick. Different types and thicknesses of the oil slicks give different Fresnel's reflection coefficients of polarized sun-glint reflections and consequently different Stokes parameters, which lead to different DOLP. We analyze the DOLP of the sun-glint reflection at the wavelength of 532 nm, and determine simultaneously the refractive index and thickness of marine oil slick from the DOLP values measured by a remote detector at two different zenith angles.

## 1. INTRODUCTION

Satellite and airborne remote sensing are important means for ocean monitoring. Marine oil spill pollution, as one of the key targets for marine monitoring, results from oil spill accident and hydrocarbon seeps. Various types of remote sensing approaches have been employed to detect the marine oil slicks. For the oil spill range detection, hyperspectral remote sensing technology has been developed for many years, mainly by detecting and analyzing the reflection spectrum of the near-infrared band generated by sunlight on the ocean surface to obtain various parameters related to oil spill [1–4]. Many ocean remote sensing databases have been established for research, such as National Oceanic and Atmospheric Administration (NOAA) class and NOAA Data Access Viewer (DAV). By studying the remote sensing data, the corresponding spillage distribution range can be obtained. Liu's team has introduced an adaptive method for automatic detection of oil spill on sea surface, which simplifies the process of manual direct operation [5]. Chen's team has shown the advantage of an airborne hyperspectral method in measuring oil spill, by using the combination of AISA and airborne hyperspectral data [6]. In [7], polarized optical remote sensing was utilized to distinguish the oil slicks from seawater within the potential critical angle range. However, they have ignored the finite thickness of the oil slicks (i.e., they have assumed that the oil slicks are infinitely thick or thick enough) and cannot classify different marine oil quantitatively, particularly for a thin oil slick.

---

*Received 26 September 2018, Accepted 12 November 2018, Scheduled 13 November 2018*

\* Corresponding author: Sailing He (sailing@jorcep.org).

The authors are with the National Engineering Research Center for Optical Instruments, Centre for Optical and Electromagnetic Research, JORCEP, Zhejiang University, Hangzhou 310058, China.

Laser induced fluorescence (LIF) can be used as a rapid method to diagnose oil spill, and many works have been reported in the recent years [8], including some commonly used methods such as fluorescence spectroscopy [9–13], infrared spectroscopy [14], gas chromatography [15], etc. Our team has also combined LIDAR and hyperspectral fluorescence technology to accurately identifying various types of oil spills [16]. It was found that the ratio between the red band at 650 nm and the green fluorescent band at 500 nm showed a good correlation with oil viscosity, while its linearity was dependent on oil density [17–19].

The thickness of an oil slick can be estimated by the intensity of the excited fluorescence, but it is vulnerable to the interference of ambient light. Therefore, a pulsed laser was adopted as the excitation light, and strong fluorescence signals could be obtained through instantaneous high fluorescence power to reduce the influence of ambient light [20]. Although the thickness of a thick oil film can be measured from the fluorescence spectrum, it is still a challenge for a thin oil slick.

In this study, we give an effective method to classify different marine oil spills by combining the polarized optical remote sensing and the inversion theory based on a thin-film optical model. Both the thickness and the refractive index of the oil slick are determined quantitatively at the same time, by analyzing the degree of linear polarization (DOLP) of oil slicks under sun-glint conditions at two different viewing angles.

## 2. MODEL ANALYSIS

### 2.1. Thin-Film Optical Model

Due to e.g., wind, the ocean surface is quite rough. We can consider the rough surface as formed by many tilted facets (see Fig. 1). In the present paper, we study how to determine the thickness and refractive index of the oil slick under the sun-glint condition. Under the sun-glint condition, only those facets (covered with the same oil layer of same thickness) tilted to a special direction would reflect the incident sunlight to the detector on the drone or satellite according to Snell's laws. Below we study the polarized sun-glint reflected locally from an oil slick of finite thickness with such a tilted facet. For simplicity, we rotate the local coordinate system so that the oil slick looks like a locally uniform layer of oil film on seawater (see Fig. 2).

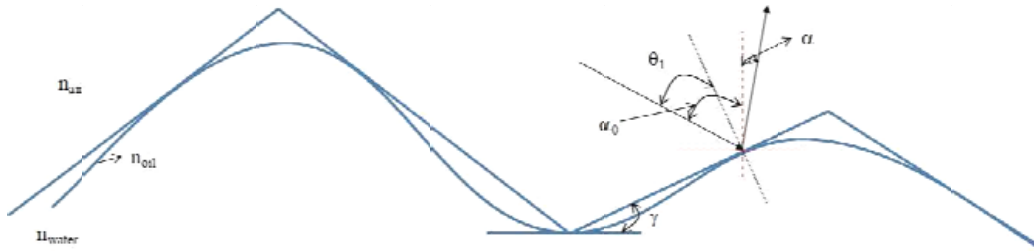


**Figure 1.** Schematic of a rough oil slick surface on the ocean.

An oil slick can be considered as a single dielectric film with a thin thickness of  $h$  on the seawater substrate (Fig. 2). This thin-film model contains air, oil slick and seawater with the corresponding refractive indices  $n_1$ ,  $n_2$  and  $n_3$ . We assume the sunlight incident on the oil slick from air with an angle  $\theta_1$  and the corresponding refraction angle is  $\theta_2$ . At the interface between the oil and seawater, the refraction angle is  $\theta_3$ . Assuming the film is very thin, we neglect the absorption of the oil. According to the thin film theory, we can easily obtain the total reflection coefficient:

$$r = \frac{r_{12} + r_{23} \exp(i * 2\delta)}{r_{12} + r_{12}r_{23} \exp(i * 2\delta)} \quad (1)$$

where  $\delta = kn_2h \cos \theta_2$  and  $k = 2\pi/\lambda$  is the wave number of the light with wavelength  $\lambda$  in the air, and  $r_{12}$ ,  $r_{23}$  are the Fresnel reflection coefficient at the corresponding interfaces between air, oil and seawater,

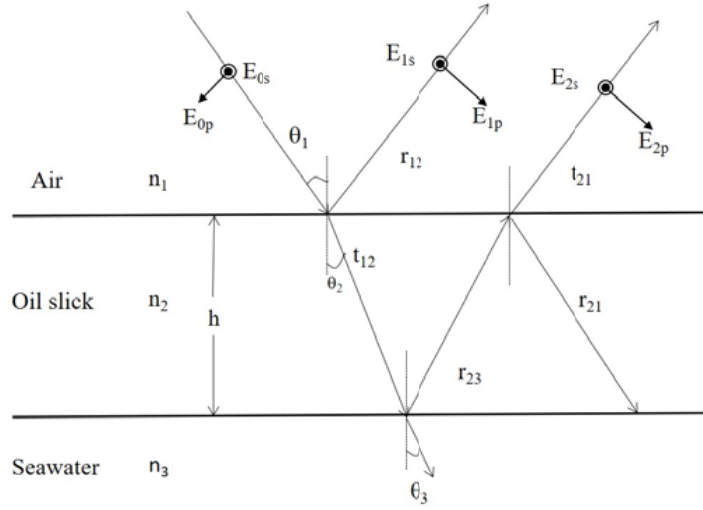


**Figure 2.** Thin-film optical model.

which can be easily found from Fresnel’s law for the orthogonal (*s*) and parallel (*p*) polarization waves, respectively:

$$\begin{cases} r_{12s} = \frac{n_1 \cos \theta_1 - n_2 \cos \theta_2}{n_1 \cos \theta_1 + n_2 \cos \theta_2} \\ r_{23s} = \frac{n_2 \cos \theta_2 - n_3 \cos \theta_3}{n_2 \cos \theta_2 + n_3 \cos \theta_3} \end{cases}, \quad \begin{cases} r_{12p} = \frac{n_2 \cos \theta_1 - n_1 \cos \theta_2}{n_2 \cos \theta_1 + n_1 \cos \theta_2} \\ r_{23p} = \frac{n_3 \cos \theta_2 - n_2 \cos \theta_3}{n_3 \cos \theta_2 + n_2 \cos \theta_3} \end{cases} \quad (2)$$

Here  $n_1 \sin \theta_1 = n_2 \sin \theta_2 = n_3 \sin \theta_3$  follows Snell’s law.

Thus, Eq. (1) can also be described as:

$$r = \frac{\zeta_2(\zeta_1 - \zeta_3) \cos \delta - i(\zeta_1 \zeta_3 - \zeta_2^2) \sin \delta}{\zeta_2(\zeta_1 + \zeta_3) \cos \delta - i(\zeta_1 \zeta_3 + \zeta_2^2) \sin \delta} \quad (3)$$

where  $\zeta_i^s = n_i \cos \theta_i$  and  $\zeta_i^p = n_i / \cos \theta_i$  ( $i = 1, 2, 3$ ) for the orthogonal (*s*) and parallel (*p*) polarization waves, respectively.

On the other hand, taking the roughness of the ocean surface into account, we can use the Cox-Munk [21–23] model to quantitatively describe the size, shape and intensity of the sun-glint pattern through a probability distribution function, which can be written as:

$$P(\alpha_0, \alpha, \varphi, \sigma^2) = \frac{1}{\pi \sigma^2} \exp\left(\frac{-\tan^2 \gamma}{\sigma^2}\right) \quad (4)$$

where

$$\tan^2 \gamma = \frac{\sin^2 \alpha_0 + \sin^2 \alpha + 2 \sin \alpha_0 \sin \alpha \cos \varphi}{(\cos \alpha_0 + \cos \alpha)^2} \quad (5)$$

Here,  $\gamma$  is the angle of the tangent plane of the rough surface with the horizontal plane;  $\alpha_0$  is the solar zenith angle;  $\alpha$  is the sensor zenith angle;  $\varphi$  is the relative azimuth angle; and  $\sigma^2$  is the surface roughness variance and can be expressed as a function of the surface wind speed  $w$  (with the unit of m/s),  $\sigma^2 = 0.003 + 0.00512w$  [21].

In addition, according to the geometrical relation, the sunlight incident angle  $\theta_1$  (same as the reflection angle) at the air-oil interface (see Fig. 1) can be written as:

$$\cos 2\theta_1 = \cos \alpha_0 \cos \alpha + \sin \alpha_0 \sin \alpha \cos \varphi. \quad (6)$$

Therefore, we can calculate the corresponding refraction angle  $\theta_2$ ,  $\theta_3$  at the air-oil interface and oil-seawater interface, respectively, according to Snell’s law.

## 2.2. Polarized Optical Model

A common way to describe a polarized light is the Stokes vector which has four components  $S = [I, Q, U, V]^T$ , where  $I$  is the total spectral radiance,  $Q$  is the spectral radiance difference between two linearly polarized lights with polarization directions along the  $x$  axis and  $y$  axis, respectively,  $U$  is the spectral radiance difference between two linearly polarized lights with polarization directions along 45 degrees and  $-45$  degrees to the  $x$  axis, and  $V$  is the spectral radiance difference between right-handed and left-handed circularly polarized lights which are defined on the Poincare sphere.

Furthermore, we can use the Mueller transformation matrix to describe the optical operation in the basis of the Stokes parameters, i.e.,

$$\begin{bmatrix} I' \\ Q' \\ U' \\ V' \end{bmatrix} = R(\eta_1) M R(\eta_2) \begin{bmatrix} I \\ Q \\ U \\ V \end{bmatrix} \quad (7)$$

where  $R$  is the rotation matrix and  $\eta_1$ ;  $\eta_2$  are the corresponding two rotation angles [24, 25]; and  $-\eta_1$  (or  $\eta_2$ ) is the angle between the scattering plane and the sensor (or solar) meridian plane under the sun-glint condition. In Eq. (7), rotation matrix  $R$  can be written as [26, 27]:

$$R(\eta) = \begin{bmatrix} 1 & 0 & 0 & 0 \\ 0 & \cos 2\eta & -\sin 2\eta & 0 \\ 0 & \sin 2\eta & \cos 2\eta & 0 \\ 0 & 0 & 0 & 1 \end{bmatrix} \quad (8)$$

and

$$\begin{cases} \tan \eta_1 = -\frac{\sin \alpha_0 \sin \varphi}{\sin \alpha \cos \alpha_0 + \cos \alpha \sin \alpha_0 \cos \varphi} \\ \tan \eta_2 = \frac{\sin \alpha_0 \sin \varphi}{\cos \alpha \sin \alpha_0 + \sin \alpha \cos \alpha_0 \cos \varphi} \end{cases} \quad (9)$$

$M$  in Eq. (7) is a transformation matrix at the interface between two isotropic, homogeneous and lossy media, which can be written as:

$$M = \frac{1}{2} \begin{bmatrix} r_s r_s^* + r_p r_p^* & r_s r_s^* - r_p r_p^* & 0 & 0 \\ r_s r_s^* - r_p r_p^* & r_s r_s^* + r_p r_p^* & 0 & 0 \\ 0 & 0 & \frac{1}{2} (r_s r_p^* + r_p r_s^*) & \frac{i}{2} (r_s r_p^* - r_p r_s^*) \\ 0 & 0 & \frac{i}{2} (r_p r_s^* - r_s r_p^*) & \frac{1}{2} (r_s r_p^* + r_p r_s^*) \end{bmatrix}. \quad (10)$$

Taking into account the roughness of the oil slick surface, Eq. (4) should be considered. Thus, the Stokes parameters can be rewritten as:

$$\begin{bmatrix} I' \\ Q' \\ U' \\ V' \end{bmatrix} = \frac{P(\alpha_0, \alpha, \phi, \sigma^2) (1 + \tan^2 \gamma)}{4 \cos \alpha} R(\eta_1) M R(\eta_2) \begin{bmatrix} I \\ Q \\ U \\ V \end{bmatrix}. \quad (11)$$

In this study, we assume that the sunlight is unpolarized, and thus the Stokes parameters are written as

$$\begin{bmatrix} I \\ Q \\ U \\ V \end{bmatrix} = \begin{bmatrix} E_s^2 + E_p^2 \\ 0 \\ 0 \\ 0 \end{bmatrix}. \quad (12)$$

Substituting Eq. (12) into Eq. (11), we can obtain the Stokes parameters of the sun-glint reflection. The DOLP (degree of linear polarization) of the sun-glint reflection is defined by

$$DOLP = \frac{\sqrt{Q'^2 + U'^2}}{I'} \approx \frac{r_s r_s^* - r_p r_p^*}{r_s r_s^* + r_p r_p^*}. \tag{13}$$

### 3. RESULTS AND DISCUSSION

According to the analysis in the previous section, the variation of the DOLP is closely related to solar zenith angle  $\alpha_0$ , sensor zenith angle  $\alpha$ , relative azimuth angle  $\varphi$  and total Fresnel reflection coefficient. Furthermore, the total Fresnel reflection coefficient of the oil slick is also related to refractive index  $n_{oil}$ , thickness  $h$  and the wavelength  $\lambda$ . We can quantitatively analyze their relationship by fixing some of these parameters. In this paper, the measurable quality is the DOLP at some viewing angles and wavelength  $\lambda = 532\text{ nm}$ . Here we ignore the attenuation coefficient difference for different oils by assuming the oil layer is ultrathin.

We first study the case when the thickness of the oil slick is fixed (here it is 100 nm as an example). When the solar zenith angle is fixed to  $30^\circ$ , Figs. 3(a)–(c) show the DOLP of the reflected sun-glint as the sensor zenith angle varies when the relative azimuth angle is fixed to  $\varphi = 0^\circ, 90^\circ, \text{ or } 180^\circ$ , and the refractive indices  $n_{oil} = 1.44, 1.54, 1.64$  and  $n_{water} = 1.34$ . In the two-beam interference model,  $n_1 = 1$  is the refractive index of the air,  $n_2 = n_{oil}$  is the refractive index of the oil and  $n_3 = n_{water}$  is the refractive of the seawater. According to Eq. (5), we can predict that the DOLP will be zero when the solar zenith angle equal to the sensor zenith angle at relative azimuth angle  $\varphi = 0^\circ$ , when the incident

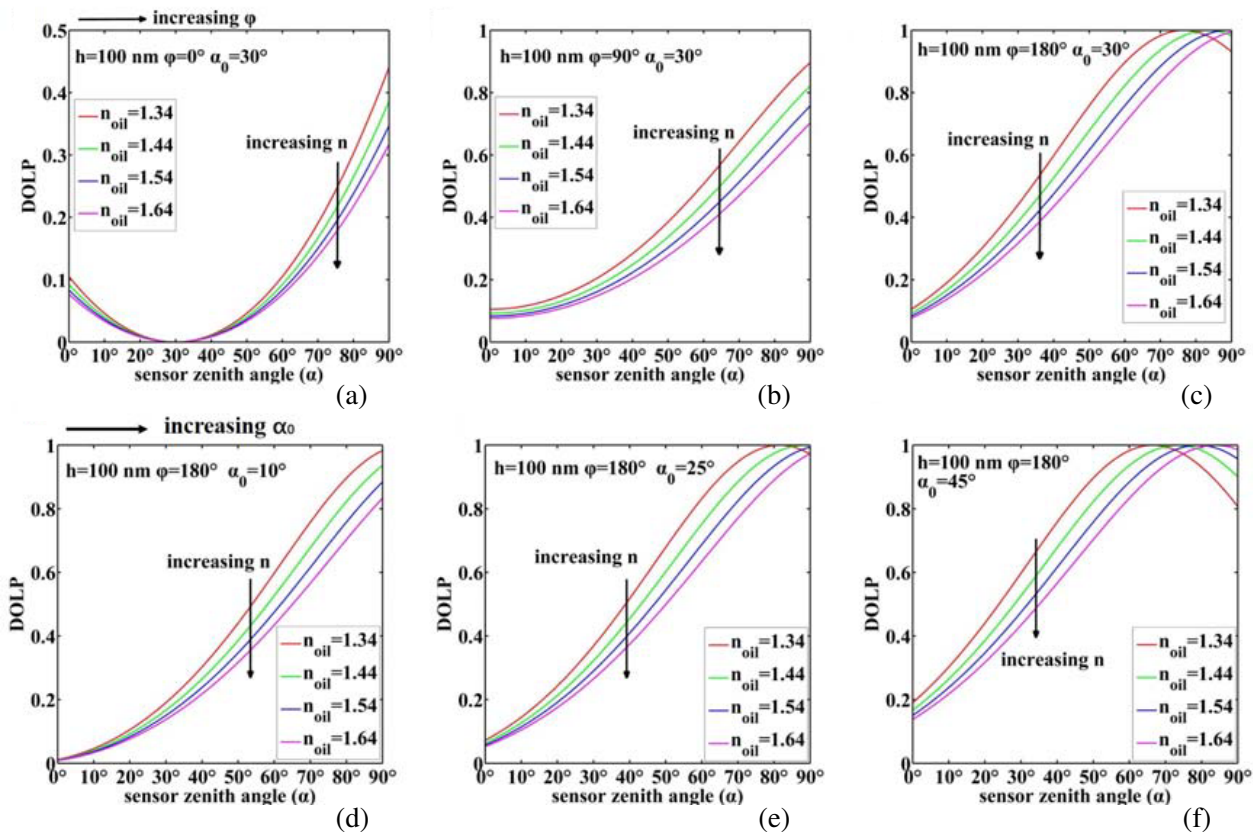


**Figure 3.** The DOLP of the sun-glint reflection from oil slicks and seawater surface with the viewing angle ranging from  $0^\circ$  to  $90^\circ$  and the refractive index ranging from 1.34 to 1.64, (a)–(c) when the thickness of the oil slick  $h = 100\text{ nm}$ ,  $\alpha_0 = 30^\circ, \varphi = 0^\circ, 90^\circ, 180^\circ$ ; (d)–(f) when the thickness of the oil slicks  $h = 100\text{ nm}$ ,  $\alpha_0 = 10^\circ, 25^\circ, 40^\circ, \varphi = 180^\circ$ .

angle  $\theta_1$  is zero, as shown in Fig. 3(a). As the relative azimuth angle increases, the Brewster angles for different oil types appear, where the DOLP equals to 1, as shown in Fig. 3(c). Furthermore, at a certain sensor zenith angle less than the Brewster angle, the DOLP decreases significantly as the refractive index increases (see Figs. 3(d)–(f)). When the relative azimuth angle is fixed to  $180^\circ$ , and the solar zenith angle is fixed to  $\alpha_0 = 10^\circ, 25^\circ$ , or  $40^\circ$ , the DOLP increases as the sensor zenith angle increases, while an opposite trend is observed when the sensor zenith angle is larger than the Brewster angle. In fact, according to Eq. (5), the larger solar zenith angle, the smaller the Brewster angle (for the sensor zenith angle) can be observed, as shown in Figs. 3(d)–(f). We can identify the category of the oil slick (i.e., the refractive index) from the variation of DOLP at a certain oil thickness.

Next, we want to study how the thickness of the oil slick influences the DOLP, assuming that we know the category of the oil slick, i.e., the refractive index is known and fixed. The results are shown in Fig. 4. At a certain sensor zenith angle less than the Brewster angle, the DOLP decreases as the thickness increases. No matter what difference DOLP may have at different values of the thickness for a specific type of oil slick, the Brewster angle is always the same, as one can see from Figs. 4(c), (e), (f): the DOLP curves for different thickness values intersect at the same point corresponding to the Brewster angle for a fixed refractive index of the oil slick. Similarly, we can determine the thickness of the oil slick from the variation of DOLP at a fixed sensor zenith angle for a certain category of oil slick (with a known refractive index).

As the thickness increases, the attenuation of light travelling through the oil film cannot be neglected, and Eq. (1) should be written as:

$$r' = \frac{r_{12} + r_{23} \exp(i * 2\delta - \beta\tau)}{r_{12} + r_{12}r_{23} \exp(i * 2\delta - \beta\tau)} \quad (14)$$

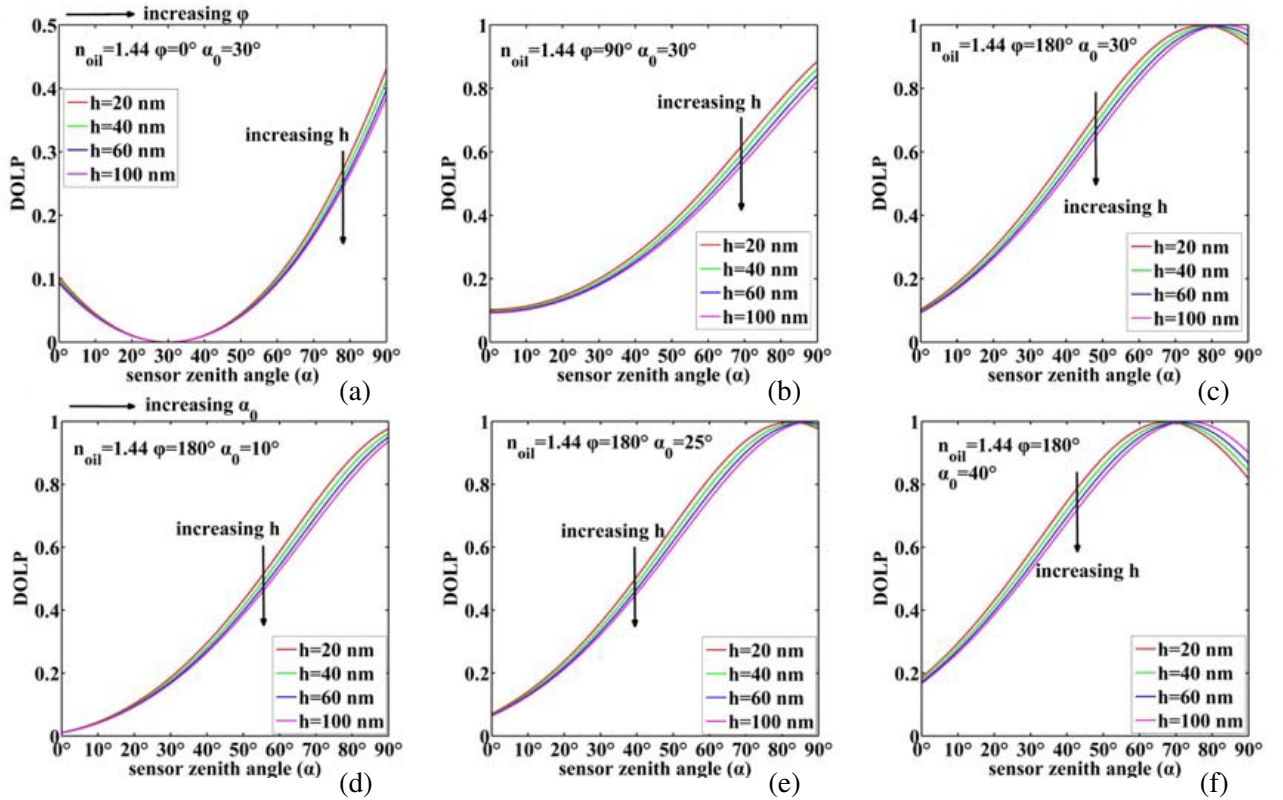


**Figure 4.** The DOLP of the sun-glint reflection from oil slicks and seawater surface with the viewing angle ranging from  $0^\circ$  to  $90^\circ$  and the oil thickness ranging from 20 nm to 100 nm, (a)–(c) when the refractive index of the oil slicks  $n_{\text{oil}} = 1.44$ ,  $\alpha_0 = 30^\circ$ ,  $\varphi = 0^\circ, 90^\circ, 180^\circ$ ; (d)–(f) when the refractive index of the oil slicks  $n_{\text{oil}} = 1.44$ ,  $\alpha_0 = 10^\circ, 25^\circ, 40^\circ$ ,  $\varphi = 180^\circ$ .

where  $\beta$  is the attenuation coefficient and  $\tau = 2 * h / \cos \theta_2$ .

We study the variation tendency of DOLP when the refractive index of the oil slick varies for different thickness values based on the thin-film optical model and the results are shown in Fig. 5(a). We define the penetration depth  $p_0$  of the oil film as, a depth where the incident light intensity decays to its  $e^{-1}$  and write the penetration depth as:  $p_0 = \cos \theta_2 / 2\beta$ . The Fresnel reflection coefficient changes cyclically with the lighthpath (the product of refractive index  $n$  and oil thickness  $h$ ) and refractive index, and consequently the DOLP changes periodically in the polarized optical model. When the oil slick is as thin as a few hundreds of nm or far smaller than the penetration depth, the oscillation period for the DOLP curve is much larger than the refractive index change range in Fig. 5(a), and consequently oscillation is not observed in Fig. 5(a) for  $d = 30$  nm and 100 nm. As the thickness becomes much larger than the penetration depth, the curves oscillate more frequently with the refractive index change and tend to approach to a smooth line (corresponding to the case of an infinitely thick oil slick).

In the meanwhile, the penetration lighthpath in the oil film can be expressed as:

$$L = n_2 p_0 = \sqrt{n_2^2 - (n_1 \sin \theta_1)^2} / 2\beta \tag{15}$$

When  $\alpha = 60^\circ$ ,  $\alpha_0 = 30^\circ$ ,  $\varphi = 180^\circ$ ,  $n_{oil} = 1.6$  and  $\beta$  is assumed to be 0.2, we can easily obtain the penetration lighthpath  $L \approx 3.6 \mu\text{m}$ . Compared with the result of DOLP calculated with the two-beam interference model [28] in Fig. 5(b), the thin-film optical model gives nearly identical result as the lighthpath becomes larger than or close to the penetration lighthpath, as shown in Fig. 5(d). However, in the case of short lighthpath, the high-order reflections cannot be ignored in evaluating the total reflection and the reflection coefficients calculated with the two-beam interference optical model is not accurate as shown in Fig. 5(c).

Finally, we try to determine the refraction index and oil thickness simultaneously from DOLP values at some discrete sensor zenith angles. Fig. 6 shows the DOLP of the sun-glint reflection from the oil slicks as the thickness or the refractive index varies at different viewing angles of the sensor when

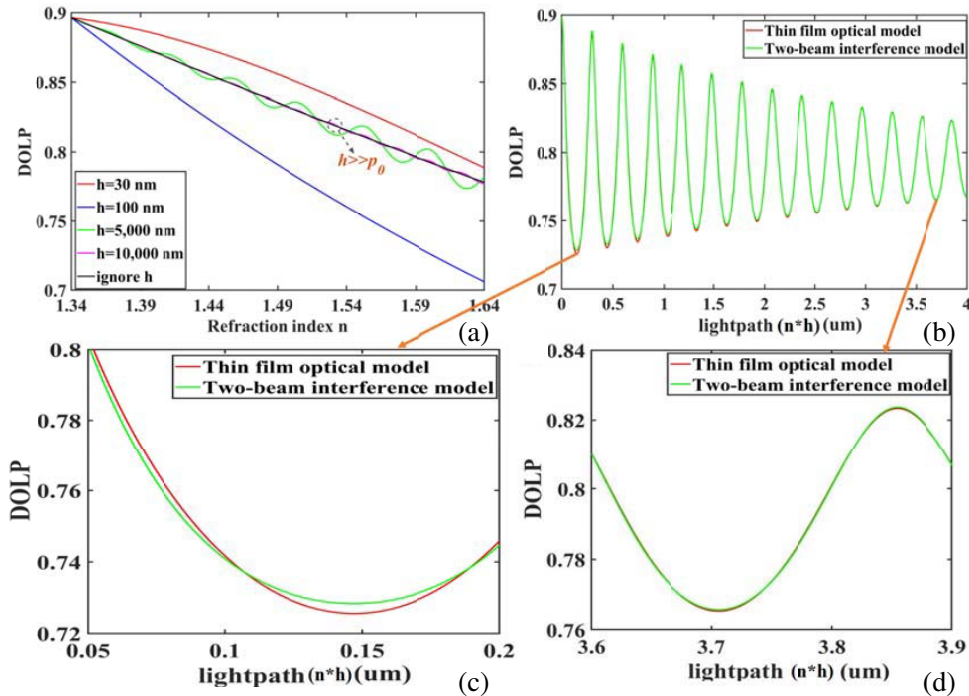


**Figure 5.** (a) The variation tendency of DOLP as the refractive index varies for oil slicks of different thickness at  $\alpha = 60^\circ$ ,  $\alpha_0 = 30^\circ$ ,  $\varphi = 180^\circ$ ; (b) The variation tendency of DOLP as the lightpath changes for different kinds of oil slicks; (c) and (d) are the locally enlarged views of (b).

the solar zenith angle and relative azimuth angle are fixed as  $\alpha_0 = 30^\circ$ ,  $\varphi = 180^\circ$ .

The phase and magnitude of the reflection coefficient would be mainly determined by the lightpath ( $n * h$ ) and the reflective index, respectively. Therefore, we will study the equi-DOLP contours as the reflective index and lightpath change. For different refraction index of the oil slick and lightpath, the DOLP values are not uniformly distributed. Furthermore, the distribution of the DOLP is distinctly different at different viewing angles of the remote sensor. We use an optical remote sensor to detect the DOLP of the sun-glint reflection at two different zenith angles and plot the corresponding equi-DOLP contours. Thus, the refraction index of the oil slick and lightpath ( $n * h$ ) could be determined simultaneously through the DOLP values measured at two different viewing angles of the sensor. As shown in Fig. 7, the equi-DOLP contours in light color correspond to the sensor zenith angle at  $60^\circ$ , and the equi-DOLP contours in bold black correspond to the sensor zenith angle at  $81^\circ$ , while the other parameters are fixed as the solar zenith angle  $\alpha = 30^\circ$ , relative azimuth angle  $\varphi = 180^\circ$ , wavelength  $\lambda = 532 \text{ nm}$ . From the intersection of two equi-DOLP contour curves, we can accurately identify the category (i.e., the reflective index) of the oil slick and lightpath (and consequently the thickness of the oil slick) at the same time. For example, if the DOLP values measured at sensor zenith angle  $\alpha = 60^\circ$  and  $81^\circ$  are 0.82 and 0.99, respectively, then the equi-DOLP contours at Fig. 7 would give the reflective index of 1.495 and a lightpath ( $n * h$ ) of  $0.0738 \mu\text{m}$  (corresponding to an oil thickness of  $48.7 \text{ nm}$ ) for the oil slick at the location of interest.

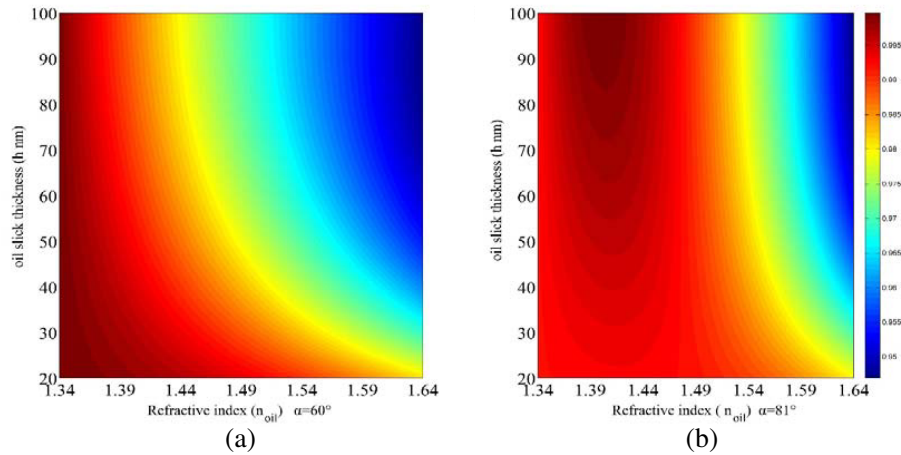


**Figure 6.** (a), (b) The color contours for the DOLP of the sun-glint reflection from oil slicks and seawater surface with the oil thickness ranging from 0 nm to 100 nm and the oil refractive index ranging from 1.34 to 1.64, under the viewing angle  $\alpha = 60^\circ, 81^\circ$ , for  $\alpha_0 = 30^\circ, \varphi = 180^\circ$ .

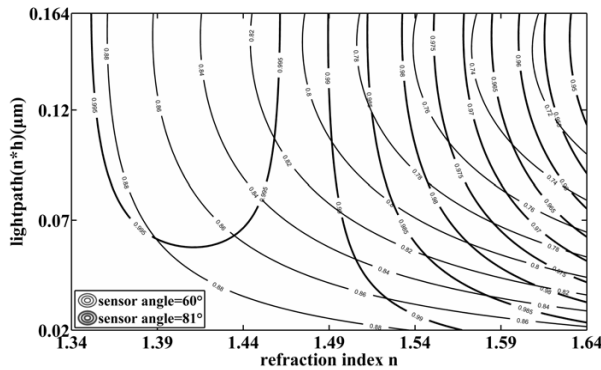


**Figure 7.** The equi-DOLP contour curves for different sensor zenith angles  $\alpha = 60^\circ$  and  $\alpha = 81^\circ$ , with the solar zenith angle  $\alpha_0 = 30^\circ$  and relative azimuth angle  $\varphi = 180^\circ$ .

#### 4. CONCLUSION

In airborne or spaceborne remote sensing technology, the DOLP of the sun-glint reflection contains some characteristic information of the oil slick on ocean surface, and can be used to determine the refractive index (corresponding to a specific type of oil) and thickness of the oil slick. In this study, we have given the polarization analysis based on the thin-film optical model, and studied the variation trend of the DOLP with the parameters of solar zenith angle, sensor zenith angle, relative azimuth angle, refractive index and thickness of the oil slick. We have found that when the thickness of the oil slick is much smaller than the penetration depth, multiple reflections of high orders cannot be ignored, and the reflection coefficients calculated with the interference of only the first two reflective beams is not accurate. We have also found that the DOLP of the sun-glint reflection is related to not only the refractive index and thickness of the oil slick, but also the detection angle. Thus, we have used the DOLP values obtained by a remote detector at two different zenith angles to identify the category and thickness of marine oil slick at the same time.

#### ACKNOWLEDGMENT

This work is partially supported by the National Key Research and Development Program of China (No. 2018YFC1407503), the Fundamental Research Funds for the Central Universities (2018FZA5001) and the National Natural Science Foundation of China (No. 11621101).

#### REFERENCES

1. Ying, L., B.-X. Liu, and P. Chen, "Study advancement in oil spill monitoring using hyper-spectral remote sensing," *Marine Environmental Science*, Vol. 31, 460–464, 2012.
2. Alam, M. S. and P. Sidike, "Trends in oil spill detection via hyperspectral imaging," *International Conference on Electrical and Computer Engineering*, 858–862, IEEE, 2013.
3. El-Rahman, S. A. and A. H. S. Zolait, "Hyperspectral image analysis for oil spill detection: A comparative study," *International Journal of Computing Science & Mathematics*, Vol. 9, No. 2, 2018.
4. Salem, F., M. Kafatos, T. El-Ghazawi, R. Gomez, and R. Yang, "Hyperspectral image analysis for oil spill detection," *Summaries of NASA/JPL Airborne Earth Science Workshop*, 5–9, Pasadena, November 2001.
5. Liu, D.-L., L. Han, and J.-Q. Zhang, "Study of automatic marine oil spills detection using imaging spectroscopy," *Spectroscopy and Spectral Analysis*, Vol. 11, 3116–3119, 2013.
6. Lei, C., R. Deng, and X. Jian, "Study on monitoring offshore platform oil spill based on Aisa + airborne hyperspectral image taking the Zhujiang River estuary as an example," *Transactions of Oceanology & Limnology*, Vol. 1, 179–184, 2009.
7. Lu, Y., Y. Zhou, Y. Liu, et al., "Using remote sensing to detect the polarized sunglint reflected from oil slicks beyond the critical angle," *Journal of Geophysical Research*, Vol. 122, No. 8, 6342–6354, 2017.
8. Baszanowska, E. and Z. Otremba, "Spectral signatures of fluorescence and light absorption to identify crude oils found in the marine environment," *Journal of the European Optical Society Rapid Publications*, Vol. 9, No. 16, 4583–4587, 2014.
9. Hagemann, H. W. and A. Hollerbach, "The fluorescence behavior of crude oils with respect to their thermal maturation and degradation," *Organic Geochemistry*, Vol. 10, No. 1, 473–480, 1986.
10. Stasiuk, L. D. and L. R. Snowdon, "Fluorescence micro-spectrometry of synthetic and natural hydrocarbon fluid inclusions: Crude oil chemistry, density and application to petroleum migration," *Applied Geochemistry*, Vol. 12, No. 3, 229–233, 1997.
11. Ryder, A. G., "Quantitative analysis of crude oils by fluorescence lifetime and steady state measurements using 380 nm excitation," *Applied Spectroscopy*, Vol. 56, No. 1, 107–116, 2002.

12. Alpern, B., et al., "Detection and evaluation of hydrocarbons in source rocks by fluorescence microscopy," *Organic Geochemistry*, Vol. 20, No. 6, 789–795, 1993.
13. Delaune, P. L., et al., "Enhanced wellsite technique for oil detection and characterization," *SPE Annual Technical Conference and Exhibition Proceedings, Formation Evaluation and Reservoir Geology*, 801–816, SPE-56802, 1999.
14. Pradier, B., et al., "Chemical basis of fluorescence alteration of crude oils and kerogens. 1. Microfluorimetry of an oil and its isolated fractions — Relationships with chemical-structure," *Organic Geochemistry*, Vol. 16, Nos. 1–3, 451–460, 1990.
15. Pharr, D. Y., et al., "Fingerprinting petroleum contamination using synchronous scanning fluorescence spectroscopy," *Ground Water*, Vol. 30, No. 4, 484–489, 1993.
16. Gao, F., J. Li, H. Lin, and S. He, "Oil pollution discrimination by an inelastic hyperspectral Scheimpflug lidar system," *Optics Express*, Vol. 25, No. 21, 25515–25522, 2017.
17. Han, Z., J. Wan, Y. Li, K. Liu, and J. Liu, "Detection method of marine oil spilling and emulsified oil based on hyperspectral imaging under UV induction," *Acta Optica Sinica*, Vol. 36, No. 1, 302–309, 2016.
18. Fingas, M. and C. Brown, "Review of oil spill remote sensing," *Marine Pollution Bulletin*, Vol. 83, No. 1, 9–23, 2014.
19. Liu, D.-Q., X.-N. Luan, J.-J. Guo, T.-W. Cui, J.-C. Jin, and R.-E. Zheng, "A small LIF remote detection system for port oil spill monitoring," *Marine Sciences*, Vol. 42, No. 1, 65–69, 2018.
20. Violetta, D., S. M. Babichenko, and L. Aleksey, "Natural water fluorescence characteristics based on lidar investigations of a surface water layer polluted by an oil film," *Oceanologia*, Vol. 44, No. 3, 339–354, 2002.
21. Cox, C. and W. Munk, "Measurement of the roughness of the sea surface from photographs of the sun's glitter," *JOSA*, Vol. 44, No. 11, 838–850, 1954.
22. Jackson, C. R. and W. Alpers, "The role of the critical angle in brightness reversals on sunglint images of the sea surface," *Journal of Geophysical Research Oceans*, Vol. 115, No. C9, 2010.
23. Zhang, H. and M. H. Wang, "Evaluation of sunglint models using measurements," *J. Quant. Spectrosc. Radiat. Transfer*, Vol. 111, 492–506, 2010.
24. Chami, M., "Importance of the polarization in the retrieval of oceanic constituents from the remote sensing reflectance," *Journal of Geophysical Research: Oceans*, Vol. 112, No. C5, 2007.
25. Harmel, T. and M. Chami, "Determination of sea surface wind speed using the polarimetric and multi directional properties of satel-lite measurements in visible bands," *Geophysical Research Letters*, Vol. 39, No. 19, L19611, 2012.
26. Priest, R. G. and S. R. Meier, "Polarimetric microfacet scattering theory with applications to absorptive and reflective surfaces," *Optical Engineering*, Vol. 41, No. 5, 988–993, 2002.
27. Diner, D. J., F. Xu, J. V. Martonchik, B. E. Rheingans, S. Geier, V. M. Jovanovic, Ab. Davis, R. A. Chipman, and S. C. McClain, "Exploration of a polarized surface Bidirectional reflectance model using the ground-based Multiangle Spectro Polarimetric Imager," *Atmosphere*, Vol. 3, 591–691, 2012.
28. Lu, Y. C., Q. J. Tian, and X. Li, "The remote sensing inversion theory of offshore oil slick thickness based on a two-beam interference model," *Science China Earth Sciences*, Vol. 54, 678–685, 2011.